IOP Publishing | Institute of Physics and Engineering in Medicine Physics in Medicine and Biology

Phys. Med. Biol. **59** (2014) 3985–4000 doi:10.1088/0031-9155/59/14/3985

Quantification of breast density using dual-energy mammography with liquid phantom calibration

Alfonso R Lam, Huanjun Ding and Sabee Molloi

Department of Radiological Sciences, University of California Irvine, CA 92697, USA

E-mail: symolloi@uci.edu

Received 24 January 2014, revised 20 May 2014
Accepted for publication 30 May 2014
Published 27 June 2014

Abstract

Breast density is a widely recognized potential risk factor for breast cancer. However, accurate quantification of breast density is a challenging task in mammography. The current use of plastic breast-equivalent phantoms for calibration provides limited accuracy in dual-energy mammography due to the chemical composition of the phantom. We implemented a breast-equivalent liquid phantom for dual-energy calibration in order to improve the accuracy of breast density measurement. To design these phantoms, three liquid compounds were chosen: water, isopropyl alcohol, and glycerol. Chemical compositions of glandular and adipose tissues, obtained from NIST database, were used as reference materials. Dual-energy signal of the liquid phantom at different breast densities (0% to 100%) and thicknesses (1 to 8 cm) were simulated. Glandular and adipose tissue thicknesses were estimated from a higher order polynomial of the signals. Our results indicated that the linear attenuation coefficients of the breast-equivalent liquid phantoms match those of the target material. Comparison between measured and known breast density data shows a linear correlation with a slope close to 1 and a non-zero intercept of 7%, while plastic phantoms showed a slope of 0.6 and a non-zero intercept of 8%. Breast density results derived from the liquid calibration phantoms showed higher accuracy than those derived from the plastic phantoms for different breast thicknesses and various tube voltages. We performed experimental phantom studies using liquid phantoms and then compared the computed breast density with those obtained using a bovine tissue model. The experimental data and the known values were in good correlation with a slope close to 1 (∼1.1). In conclusion, our results indicate that liquid phantoms are a reliable alternative for calibration in dual-energy mammography and better reproduce the chemical properties of the target material.

Keywords: dual-energy mammography, breast density, liquid phantoms, plastic phantoms, thickness ratio

(Some figures may appear in colour only in the online journal)

1. Introduction

Breast cancer is one of the most common cancers and is the leading cause of death in women worldwide (World Health Organization 2006). X-ray mammography currently is the standard tool in breast cancer screening. Breast density is defined as the ratio of glandular tissue over the whole breast. Increased breast density has been shown to have a strong correlation with breast cancer risk (Wolfe 1976, Boyd *et al* 1998, 2007, Wolfe *et al* 1987, Byrne 1997, Shepherd *et al* 2002). Wolfe, who originally reported this correlation, used a qualitative classification to cluster breast images into risk categories (Wolfe 1976, Sickles 2007). In subsequent years, different quantitative and geometrical approaches to estimate breast density have been developed. A number of these approaches involve segmentation of image gray levels. Within the boundary of the breast, the image was segmented, and a projected area of these pixels was computed (Byng *et al* 1994, 1996, 1998, Heine and Velthuizen 2000, Lu *et al* 2007, Zhou *et al* 2001). However, the previous approaches assumed the pixels in the breast images could be classified into either 100% glandular or 100% adipose tissues, which potentially leads to inaccurate breast density measurements, because different thicknesses could generate similar results. Furthermore, the 3D nature of the breast was not taken into account in this approach.

Volumetric-based methods came as a natural continuation to overcome the limitations of area-based techniques. They intended to initially calibrate imaging systems using tissue-equivalent phantoms and subsequently correct variations in exposure during image acquisition (Highnam *et al* 1996, 2006, 2007, Pawluczyk *et al* 2003). However, these techniques depend on the knowledge of breast thickness to measure breast density. The breast thickness estimation is limited by the assumptions required in the breast shape model and the errors associated with the paddle thickness measurement (Ducote and Molloi 2010a).

Dual-energy imaging has previously been used in contrast-imaging and calcification imaging (Johns *et al* 1985, Johns and Yaffe 1985, Marziani *et al* 2002, Taibi *et al* 2003, Kappadath and Shaw 2005, 2004, Lemacks *et al* 2002). Recently, studies have reported the use of these techniques in the quantification of breast density and the estimation of the glandular and adipose thicknesses. This is done by exploiting the variety of chemical elements with different atomic numbers Z present in the tissues (Ducote and Molloi 2008, 2010a). Although good correlations between the measured and known densities were reported, the measured values were out of the realistic breast density range of 0% to 100% (Ducote *et al* 2011). This problem was attributed to the use of breast-equivalent plastic phantoms during the calibration process in dual-energy mammography. The chemical composition of these phantoms consists of common elements that can be found in breast tissue, such as hydrogen, carbon, nitrogen, oxygen, and small fractions of heavy elements such as Cl and Na. The phantoms were primarily designed to match the attenuation characteristics of glandular and adipose tissues for conventional single kVp spectra, and were intended for calibrating an automatic exposure control devices with single energy mammography applications. However, plastic phantoms may not provide an accurate measure of the breast tissue attenuation coefficients for different energies. Thus, they are not good calibration materials for breast density quantification with dual-energy mammography. The main reason is that the mass fractions of their chemical

composition differ from those of the real breast since the design of these plastic phantoms was based on the chemical composition from Hammerstein *et al* (1979), which has a large range of variations.

Ducote *et al* (2011) performed dual-energy mammography studies with plastic calibration phantoms using a bovine model and found significant differences between measured and predetermined volumetric density. Thus, it is important to create phantoms that are able to closely reproduce the physical attenuation properties of the breast.

A possible solution to overcome the limitations of the plastic phantoms is to develop calibration phantoms with elemental chemical composition comparable to breast tissue. Both glandular and adipose tissues are composed primarily of hydrogen, carbon, nitrogen, and oxygen. Heavy elements are present in negligible concentrations. Based on that rationale, the implementation of liquid phantoms can be a suitable approach.

The aim of our study is to investigate the implementation of liquid phantoms in dual-energy imaging to improve the quantification of breast density. We first designed calibration phantoms composed of liquid compounds that match the mass ratios of hydrogen, carbon, nitrogen, and oxygen in glandular and adipose tissues, respectively. Three liquids were chosen for this study: water, glycerol, and isopropyl alcohol. A proper proportion of each of these liquids forms a reliable mixture that mimic the properties of each reference material (Jennings 1993). A dual-energy mammography simulation protocol was implemented for the liquid phantoms. Breast density was measured based on the low- and high-energy signals using both liquid and plastic calibration phantoms. Thicknesses of glandular and adipose tissues were measured using a higher order fitting polynomial function. The values of these thicknesses were used to measure breast density, and then compared to the known breast density values. Experimental studies with *ex-vivo* tissue samples were performed previously (Ducote *et al* 2011). Using the fitting coefficients from liquid calibration phantoms, we measured the experimental breast densities values and compared to the values reported in literature using CIRS phantom.

2. Theory

The ultimate goal of the simulation was to determine the proportion of liquid compounds required for designing breast-equivalent phantoms. The procedure is described in a study by Jennings (1993). If the linear attenuation coefficient of a reference material μ_0 and its thickness t_0 are known, they can be modeled as a combination of linear attenuation coefficients μ_i from different materials with their respective thicknesses $t_i$using the mathematical relation:

$$\mu_0 t_0 = \sum_{i=1}^{N} \mu_i t_i. \tag{1}$$

If the thicknesses t_i of materials i are combined to the reference thickness t_0:

$$k = \sum_{i=1}^{N} a_i = \text{constant}; \; a_i = \frac{t_i}{t_0}. \tag{2}$$

The attenuation coefficient μ_0 is quantified by determining an optimal set of thickness ratios a_i, which depends on the number of materials involved. The constant k depends on the volume of the reference material, and is not a sum of the volumes of the liquid materials involved, since volume change occurs when liquids are mixed. The equations above can be used for the mixtures of two or three materials. In cases when more materials are involved more variables are added, and more equations will have to be solved. Two materials were used in the experimental setting studied by Alvarez and Macovski (1976) and

Lehmann *et al* (1981). In the case of three materials, a third equation is required to determine the thickness ratio a_i. Thus, the derivative of equation (1) with respect to the photon energy appears as:

$$\mu_0' t_0 = \sum_{i=1}^{N} \mu_i' t_i. \tag{3}$$

Combining equations (1)–(3), the set of thickness ratios of the three materials are determined as a function of their attenuation coefficients:

$$a_1 = \frac{t_1}{t_0} = \frac{[\mu_2'(\mu_0 - k\mu_3) + \mu_3'(k\mu_2 - \mu_0) + \mu_0'(\mu_3 - \mu_2)]}{\mu_1'(\mu_3 - \mu_2) + \mu_2'(\mu_1 - \mu_3) + \mu_3'(\mu_2 - \mu_1)} \tag{4}$$

$$a_2 = \frac{t_2}{t_0} = \frac{[\mu_3'(\mu_0 - k\mu_1) + \mu_1'(k\mu_3 - \mu_0) + \mu_0'(\mu_1 - \mu_3)]}{\mu_1'(\mu_3 - \mu_2) + \mu_2'(\mu_1 - \mu_3) + \mu_3'(\mu_2 - \mu_1)} \tag{5}$$

$$a_3 = \frac{t_3}{t_0} = \frac{[\mu_1'(\mu_0 - k\mu_2) + \mu_2'(k\mu_1 - \mu_0) + \mu_0'(\mu_2 - \mu_1)]}{\mu_1'(\mu_3 - \mu_2) + \mu_2'(\mu_1 - \mu_3) + \mu_3'(\mu_2 - \mu_1)}. \tag{6}$$

The attenuation coefficients of a material are associated with their cross sections $\left(\frac{\mu}{\rho} \sim \sigma\right)$ which are computed using a higher-order polynomial fitting function:

$$\log(\sigma) = \sum_{i=0}^{3} A_i (\log E)^i \tag{7}$$

where σ is the total cross section of the material, A_i are the fitting coefficients of the polynomial function previously determined, and E is the photon energy (McMaster *et al* 1969).

In the simulation protocol, the total cross section σ has three components: photoelectric effect, Compton, and Rayleigh scattering. Each of these components has its own set of fitting coefficients A_i. Using equation (7) and its first derivative, μ_i and μ_i' are computed, a set of thickness ratios (a_1, a_2, a_3) at each energy E for a given k is determined. Each set of thickness ratios is used to compute the linear attenuation of the target-equivalent material. The set that provides the smallest error is chosen as the optimal set of thickness ratios (or the best k), which gives the proportion of liquids required to create the reference material-equivalent mixture. The mixture is decomposed in their basic chemical elements (hydrogen, carbon, and oxygen) and their mass fractions are used in the dual-energy decomposition simulation to calculate the breast density.

3. Methods

3.1. Design of breast-equivalent liquid phantoms in simulation

The chemical composition of the liquid phantoms was determined using computational simulation based on the theoretical foundations described above. Three liquid materials were chosen to create breast-equivalent phantoms: water (H_2O), glycerol ($C_3H_8O_3$), and isopropyl alcohol (C_3H_8O). These materials are miscible, low cost, and easy to obtain and handle in the laboratory. From the simulation results, a set of optimal thicknesses ratios $(a_{\text{water}}, a_{\text{glycerol}}, a_{\text{isopropyl}})$ was determined and used to estimate the amount of these liquids required to create each of pure glandular and pure adipose tissue equivalent liquid phantoms. The flexibility of the liquid phantoms allows exploration of a wide range of densities and thicknesses by mixing the glandular and adipose-equivalent liquid phantoms proportionally.

In the simulation, 11 different breast density values (from 0% to 100% at 10% step) were used. Eight different breast thicknesses (1–8 cm at 1 cm step) were investigated for each breast

density, making a total of 88 calibration points that were used to compute the low- and high-energy signals. The elemental chemical composition data for glandular and adipose tissues from the NIST database were used as reference materials to design the liquid phantoms.

3.2. Simulating the detector signals

The simulated detector signal S computed in this study has the form:

$$S = \int f^2 N_0(E)\, \mathrm{e}^{-\mu_f(E)t_f}\, \mathrm{e}^{-(\mu_a t_a + \mu_g t_g)} W(E) Q(E) G(E)\, \mathrm{d}E. \tag{8}$$

Equation (11) models the signal generated by a digital mammographic device used in this study (Ducote and Molloi 2010a, 2008) (Selenia Hologic Inc., Bedford, MA). The size of the aperture, f^2, was set at 0.0049 mm^2. $N_0(E)$ is the incident x-ray spectrum in the absence of material, which is simulated using the TASMIP algorithm (Boone and Seibert 1997).

A pre-patient filtration factor, $\mathrm{e}^{-\mu_f(E)t_f}$, is used, which varied between the low- and high-energy spectra. The terms $\mu_i(E)$ and t_i $(i = a, g)$, in the attenuating term, $\mathrm{e}^{-(\mu_a t_a + \mu_g t_g)}$, stand for the linear attenuation coefficients at energy E and thickness of tissue material i, respectively. These terms are computed using the algorithm designed by Boone and Chavez (1996). $W(E)$ is the energy weighting factor that characterizes the detector type, $Q(E)$ is the quantum detection efficiency of the detector, and $G(E)$ is the absorption due to the presence of cellular x-ray scatter grid. Details about how $G(E)$ was measured are described in Ducote and Molloi (2008). Since we are simulating the properties of an amorphous selenium photoconductor in a digital mammography device, we set $W(E) = E$, and $Q(E)$ were calculated for a 200 μm selenium absorber. In this study, the tube voltage was set at 28 kVp with a filter of 50 μm rhodium (Rh) and 49 kVp with a filter of 300 μm of copper (Cu) for the low- and high-energy exposures, respectively.

3.3. Quantification of breast density

In dual-energy imaging, different materials in a sample are distinguishable through their differential attenuations as a function of energy. To make such distinction, two separate x-ray intensity measurements are made with different x-ray spectra (two exposures with different kVp, low and high energy). The detector measures the low- and high-energy transmitted intensities of the x-ray beams, $S_l(t_i)$ and $S_h(t_i)$. Those variables are line integrals of the attenuation and are functions of the thicknesses of the i materials in the object. Regarding the breast, these thicknesses correspond to the glandular and adipose tissue thicknesses t_g and t_a, respectively. Thus, a set of equations is defined:

$$\begin{pmatrix} \mu_a^l & \mu_g^l \\ \mu_a^h & \mu_g^h \end{pmatrix} \begin{pmatrix} t_a \\ t_g \end{pmatrix} = \begin{pmatrix} S^l \\ S^h \end{pmatrix}. \tag{9}$$

By inverting $S_l\left(t_g, t_a\right)$ and $S_h\left(t_g, t_a\right)$, t_g and t_a can be determined. However, due to the non-linearity caused by x-ray scatter and beam hardening, the computation of these thicknesses is not a straightforward task (Brody *et al* 1981). A non-linear rational polynomial function reported previously (Ducote and Molloi 2010a) was used to compute the thicknesses t_g and t_a:

$$t_i = \frac{a_0 + a_1 l + a_2 h + a_3 l^2 + a_4 lh + a_5 h^2}{1 + b_1 l + b_2 h} \quad i = g, a. \tag{10}$$

The terms l and h stand for the logarithms of the low- and high-energy signals, respectively. These signals are divided by their respective open-field signals (absence of material). As

mentioned above, 88 calibration points were used to determine the set of fitting coefficients that estimates the thicknesses of glandular (t_g) and adipose (t_a), respectively. Finally, breast density was defined as:

$$\mathrm{BD} = \frac{t_g}{t_g + t_a}. \tag{11}$$

The feasibility and robustness of the fitting parameters were tested by implementing them to an additional test set of 88 thicknesses for glandular and adipose tissues. The thicknesses in the test set were not used in the fitting procedure but were within the fitting range. In this study, BD is expressed in percentage of glandular tissue present in the sample.

3.4. Liquid and plastic phantom comparison

Once the elemental chemical composition of liquid phantoms is determined, the dual-energy signals at low and high energies can be computed as described section 3.3. In order to validate the quality of the results from liquid phantoms, elemental chemical composition of plastic phantoms (CIRS, Norfolk, VA) obtained from literature was implemented in the simulation to compute their respective low- and high-energies signals. The thicknesses of glandular and adipose tissues were estimated using the logarithm of the low- and high-energies signals into equation (8). Two sets of fitting coefficients were computed, one set that comes from liquid phantoms and another set from plastic CIRS phantoms. These sets of fitting coefficients were used in the reference dual-energy signals to measure the thicknesses and breast densities. Linear correlation is expected between known and measured densities.

3.5. Simulated tube voltage change

In clinical applications, the tube voltage at low energy is usually modified according to the thickness of the patient's breast. If phantoms are used for calibration purposes, they must provide reliable calibration parameters at various tube voltages, and therefore the linear correlation between measured and known density should provide a stable slope. To test the robustness of the slopes obtained from liquid and plastic phantoms, the breast phantom densities at different low-energy signals were computed. Four different voltages for low energy were used: 20, 28, 32, and 35 kVp. Breast phantom densities and thicknesses were measured using the previously defined 88 calibration points. The obtained results were compared to the known values.

4. Experimental setting

4.1. Ex-vivo samples

Ex-vivo samples based on bovine lean and fat tissues were prepared and used in image acquisition in a previous study (Ducote *et al* 2011). In this study (Ducote *et al* 2011), it was determined that the chemical compositions of the bovine adipose and lean tissues are similar to those of the human adipose and skeletal muscle tissues reported in the NIST database. Thus, we used them as reference materials to design liquid phantoms that mimic the properties of breast tissues. *Ex-vivo* samples were prepared using pure lean muscle and pure fat and cut into cubes of approximately 1 cm^3 in volume. The parameter of interest is the volumetric lean percentage (VLP), which is the relative amount of lean contained in a sample where lean and fat are present in a sample. Each sample had a total mass of 500 g. VLP was varied from 0 to 100%, in increment of 10%, for a total of 12 measurement points. Additional details about the preparation and manipulation of these samples are described elsewhere (Ducote *et al* 2011).

4.2. Liquid phantom preparation

The amounts of the liquid ingredients to prepare the bovine-equivalent liquid phantoms were determined as described above. High precision pipets were used to accurately measure the volume of different liquids before mixing them in glass flasks. Two mixtures were created, one to represent lean tissue (100% muscle) and the other one for adipose (0% muscle). The mixtures were placed in sealed plastic containers for image acquisition.

The mixtures were used to create a set of liquid phantoms at different densities. In our experimental study, we used the following densities: 0, 30, 50, 70 and 100% with the total thicknesses of 2, 3, 4, 5, 6, and 8 cm, measured on the x-ray beam propagation plane. These phantoms were placed in polystyrene containers for image acquisition. The dimension of each container was $10.21 \times 3.83 \times 11.76\ \text{cm}^3$.

4.3. Image acquisition and processing

All images were acquired using a digital mammography system (Selenia, Hologic, Inc, Bedford MA). The configuration of this system consists of two beam filters: a 50 mm Rh filter and a 300 mm Cu filter, for the low- and high-energy exposures, respectively. An amorphous selenium direct conversion detector is used with a tungsten x-ray tube. In this study, dual-energy images were acquired at 28 and 49 kVp with 24 and 4 mAs, respectively.

Dark-field images were acquired, and used to correct the low- and high-energy images. The resulting images were then normalized by their corresponding open-field images before log transformation. Since the liquid phantom was contained in plastic containers, open-field images with empty containers at the same location of the phantoms were acquired and used to remove the contribution of the plastic containers in the log signals. The low- and high-energy images were corrected for scatter before decomposition (Ducote and Molloi 2010b).

A region of interest (ROI) was drawn in the phantom area. The mean values obtained from the ROIs for the low- and high-energy images were used to estimate the thicknesses of glandular- and adipose-equivalent tissues contained in the phantom.

The calibration coefficients were then applied on dual-energy signals from the *ex-vivo* sample to estimate the bovine lean and adipose thicknesses. Since the bovine lean and adipose thicknesses were computed from the dual-energy images, we measured the VLP using the fitting coefficients obtained from both liquid and plastic phantoms and compared the results with the known VLP.

5. Results

5.1. Simulation

5.1.1. Elemental chemical composition of breast-equivalent phantoms. Using the data for glandular and adipose human tissues from the NIST database (Hubbell and Seltzer 1995) as reference materials, we used the simulation protocol to quantify the amount of liquids necessary to design glandular- and adipose-equivalent phantoms. The percentage compositions of liquid phantoms for glandular and adipose are shown in table 1. We can observe that the chemical composition for each tissue differs significantly. In adipose, the contribution of water is less than 2%, when glycerol and isopropyl alcohol contribute around 14% and 85%, respectively. For glandular, the water, isopropyl and glycerol contributions are 43%, 35% and 23%, respectively. This result is expected, because there is always a small amount of water in adipose tissue. Since these liquid materials are composed of hydrogen, carbon, and oxygen, we decomposed them in terms of the mass fractions of basic chemical elements, and compared

Table 1. Percentages of liquid compounds to create breast-equivalent liquid phantoms predicted by simulations. Chemical compositions of adipose and glandular were obtained from NIST database.

Tissue	Water (%)	Glycerol (%)	Isopropyl (%)
Adipose	1.49	13.90	84.61
Glandular	42.68	22.62	34.69

them with the reference materials from NIST database and the CIRS plastic phantoms. The mass percentages are shown in figure 1.

Note that adipose and glandular-equivalent liquid phantoms have similar amounts of carbon and oxygen, while their corresponding equivalent CIRS phantoms are significantly different. The hydrogen component is comparable among all of the phantoms. CIRS has nitrogen and heavier elements that are not present in the liquid phantoms.

The linear combination of the attenuations of the liquid compounds gave rise to the linear attenuation of the reference materials. We have also considered the linear attenuation of the reference materials using the CIRS chemical composition (Ducote *et al* 2011). In figure 2 (top panels), we observe that the linear attenuations of the adipose and glandular tissue equivalent phantoms generated by the simulation protocol show slight differences with respect to the values reported in the NIST database. The linear attenuation coefficients for glandular tissue show small variations in both liquid and plastic phantoms. Adipose-equivalent liquid phantoms show a better correlation in its linear attenuation coefficients than those from the CIRS phantoms. This can be seen from the difference between linear attenuation computed using the mass fractions from the phantoms and the linear attenuation given by NIST. They are displayed in the bottom panels of figure 2. For glandular tissue, both phantoms give smaller percentage error but within the range of 20–40 keV, liquid phantoms provide lower percentage errors than that of CIRS plastic phantoms. In the case of adipose tissue, plastic phantoms give smaller errors at energies >40 keV than liquid phantoms.

5.1.2. Measurements of breast density. A set of test points was used to measure the breast density and check the reliability of the fitting coefficients using simulation. The results are shown in figure 3. Note that the error in percentages in most of the test points did not exceed 0.05%. RMSE for the liquid and plastic phantoms were 0.0100% and 0.0115%, respectively. These results indicate that the fitting coefficients are suitable to measure the thickness and density of reference materials.

Using the fitting coefficients and the values of the signals for low and high energy in equation (10), we measured the thicknesses of glandular and adipose tissues. With these measured thicknesses, we used equation (11) to compute the *measured density* for each total thickness considered in this study. As an illustration, the results for the total breast thickness of 5 cm are shown in figure 4. The simulated *known density* is computed using the thicknesses of glandular and adipose tissues that were initial inputs for equation (8), previously known by the observer. In the *ex-vivo* experiment the known density is computed by determining the amount of lean contained in a sample of lean and fat (Ducote *et al* 2011), and the measured density is computed by taking the fitting coefficient from the calibration phantoms and apply it to the image data to generate the measured density.

In figure 4 both liquid and CIRS phantoms show good correlation with respect to the known breast density. The results from the plastic phantom show a slope of 0.6, while the

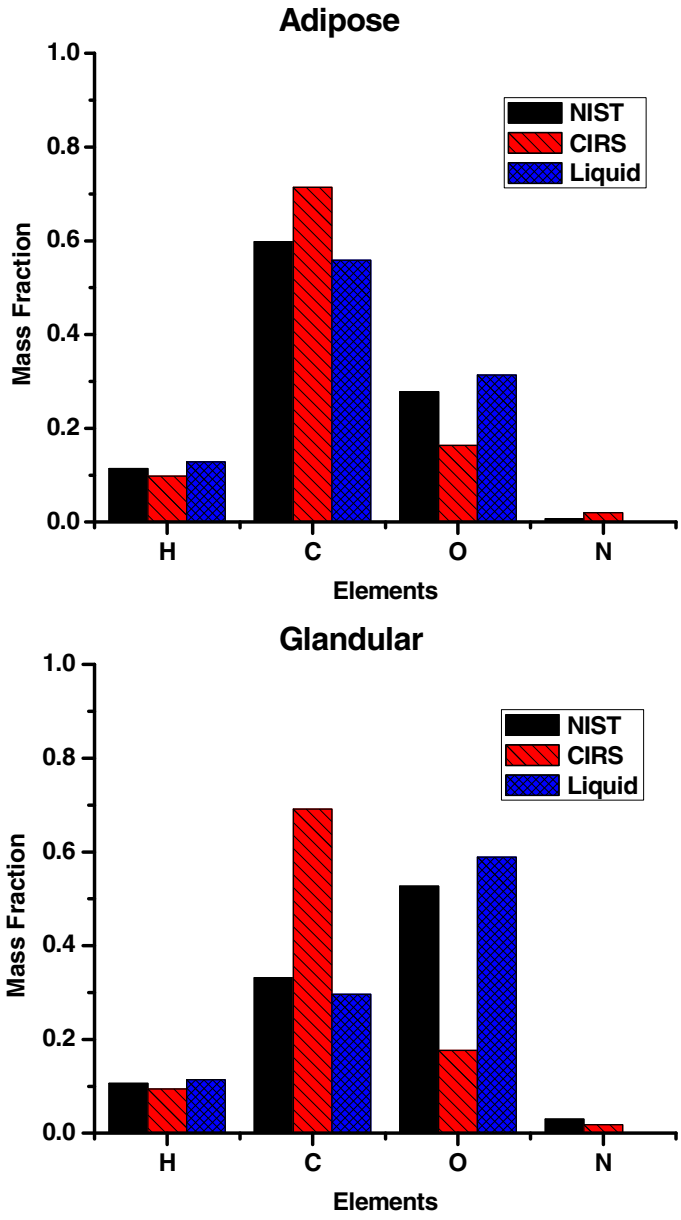

Figure 1. Comparison of elemental chemical compositions of the adipose and glandular tissues from NIST database to CIRS and liquid phantoms.

results obtained from liquid phantoms shows a slope close to 1. However, in both cases there is a non-zero intercept of approximately 7%.

To simulate a clinical application of dual-energy mammography, the tube voltage for the low-energy image was increased with increasing breast thickness. The same set of calibration points was used, and the breast density and tissue thickness were computed. To easily visualize the slope variations when tube voltage is changed, the measured densities at 20 kVp were used

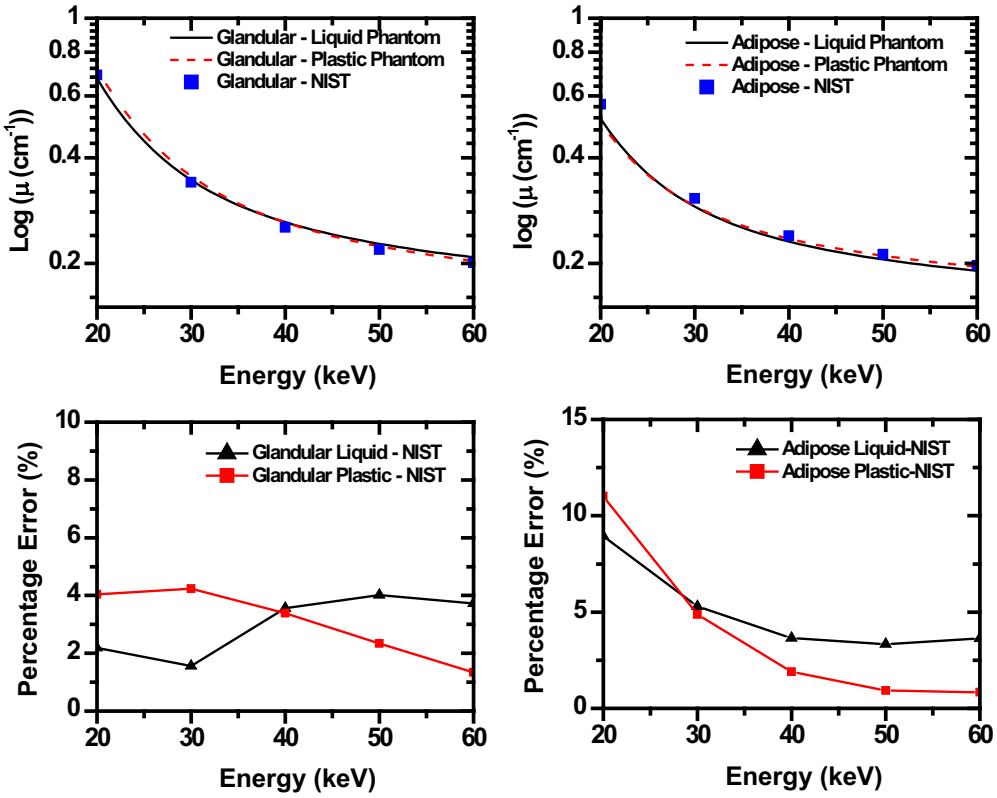

Figure 2. Comparison between simulated linear attenuation coefficients of the adipose and glandular tissues using liquid phantoms and CIRS phantoms chemical composition to the coefficients reported in the NIST database.

to normalize the results obtained from the rest of the tube voltages. The results are shown in figure 5. Note that for liquid phantoms, the normalized slope increases less than 1% when the tube voltage was increased. For the CIRS phantoms, the normalized slope changed up to 5%. At different thicknesses, liquid phantoms seem to perform well to keep the slope steady with slight variations, while for CIRS phantom the deviations were higher. The slope computed using CIRS phantoms shows variations at different thicknesses for 28 kVp beam. Those variations were higher for higher thicknesses.

5.2. Experimental phantom study

The elemental chemical composition of the liquid phantoms was compared to the reference materials (skeletal muscle and adipose) and plastic phantoms in table 2. The mass fractions for the skeletal muscle tissue show that the muscle-equivalent liquid phantom should be composed of hydrogen (11.2%), oxygen (88.6%) and a small fraction of carbon (0.2%), which comes mainly from water with a small amount of isopropyl alcohol. The reason that glycerol is not necessary in this case is that the ratios of hydrogen and oxygen in skeletal muscle are similar to those in water (10% and 70%, respectively). The slight difference is compensated by addition of isopropyl alcohol.

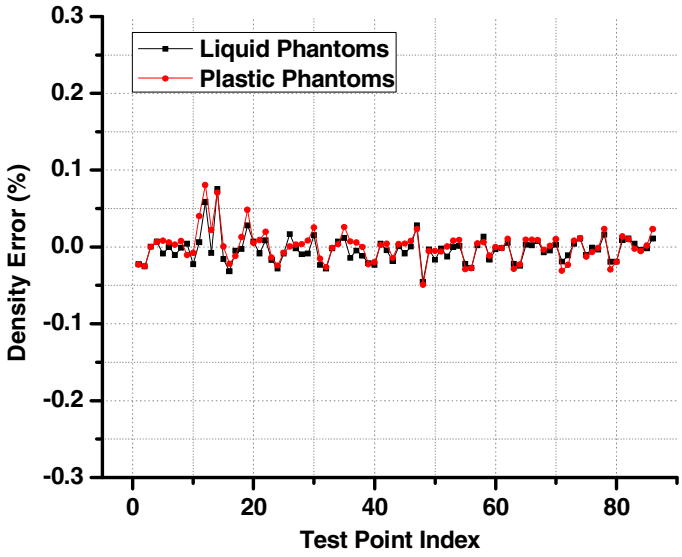

Figure 3. Density errors in percentage between measured and known densities for the set of test points in both liquid and plastic phantoms.

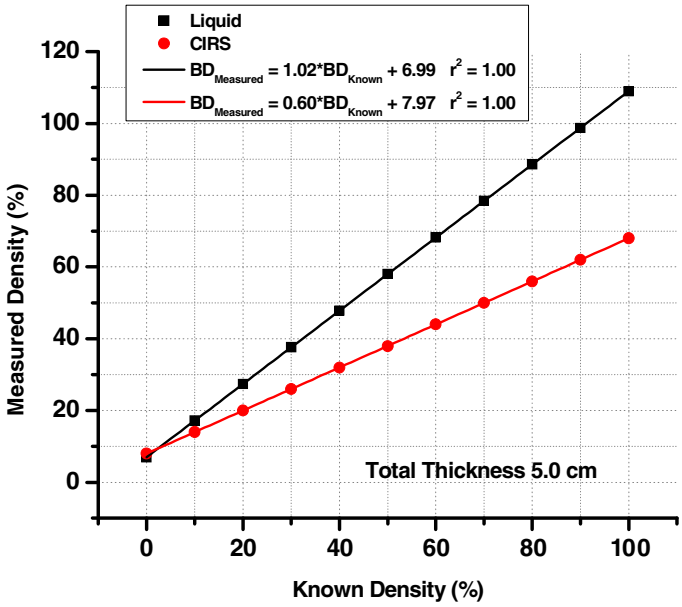

Figure 4. Measured density versus known density for a total breast thickness of 5 cm. Measured density for liquid and CIRS phantoms were computed by obtaining the thicknesses of adipose and glandular tissues from NIST. The adjusted r^2 for both phantoms is 1.

The hydrogen content in the liquid phantom is comparable to those in the reference material and CIRS plastic phantom. The amounts of oxygen and carbon in the reference material are approximately 33% and 55%, respectively. In the case of plastic phantoms, the amounts of carbon and oxygen differ by a factor 2 and 0.3, respectively, if compared to

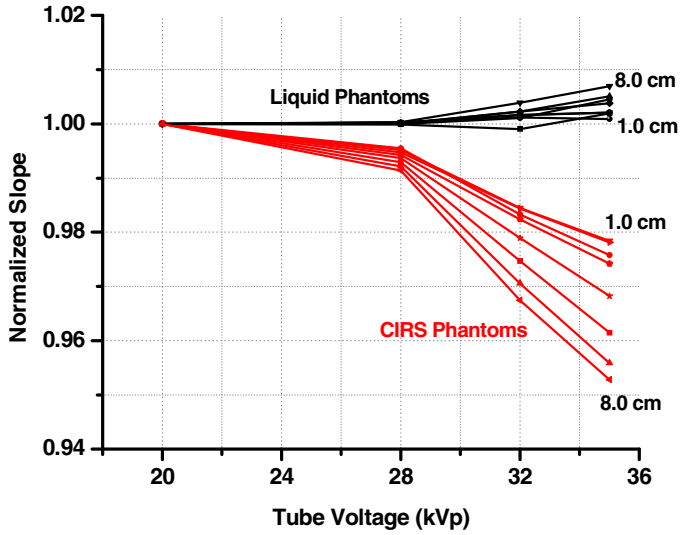

Figure 5. Slopes of measured and known densities for liquid and CIRS phantoms computed at different tube voltages and total breast thicknesses. The slope computed at 20 kVp was used as a normalization factor.

Table 2. Mass fractions of the chemical elements for the materials used in the experimental study.

Tissue	H	C	O	N	Other (Na, Ca, Cl, P, S, K)
NIST glandular	0.1060	0.3320	0.5270	0.0300	0.0005
NIST muscle	0.1020	0.1430	0.7100	0.0340	0.0110
CIRS glandular	0.0941	0.6913	0.1766	0.0184	0.0030
Liquid muscle	0.1120	0.0018	0.8863		
NIST adipose	0.1140	0.5980	0.2780	0.0070	0.0030
CIRS adipose	0.0978	0.7141	0.1634	0.0201	0.0038
Liquid adipose	0.1282	0.5583	0.3135		

the amounts reported for the reference material. The mass fractions for the adipose tissue show comparable amounts of these elements. Overall, these results match well with those of experimental chemical decomposition based on water, lipid and protein reported in Ducote *et al* (2011). They reported that the bovine adipose tissue is chemically similar to the human adipose tissue.

Bovine model-equivalent liquid phantoms at different known thicknesses and densities were used as calibration to acquire images at low and high energy. The computed low- and high-energy signals obtained from these images were used to predict the adipose and lean tissue thicknesses and densities. The computed fitting coefficients were then used to estimate VLP. The results are shown in figure 6.

As expected, a strong linear correlation was observed between the measured and known VLP when liquid and plastic phantoms were used. When fitting coefficients from liquid phantoms were used, a slope of 1.1 and intercept of 3.71% were obtained. These values are very close to the values predicted in the simulation (1.05 and 3.35%, respectively). On the other hand, in the case of using the fitting coefficients from plastic phantoms, the slope and intercept were 1.53 and 7.49%, respectively. Although this result carries out the same conclusion as in the simulation, they differ slightly from the expected values of 1.35 and 6.88%, respectively.

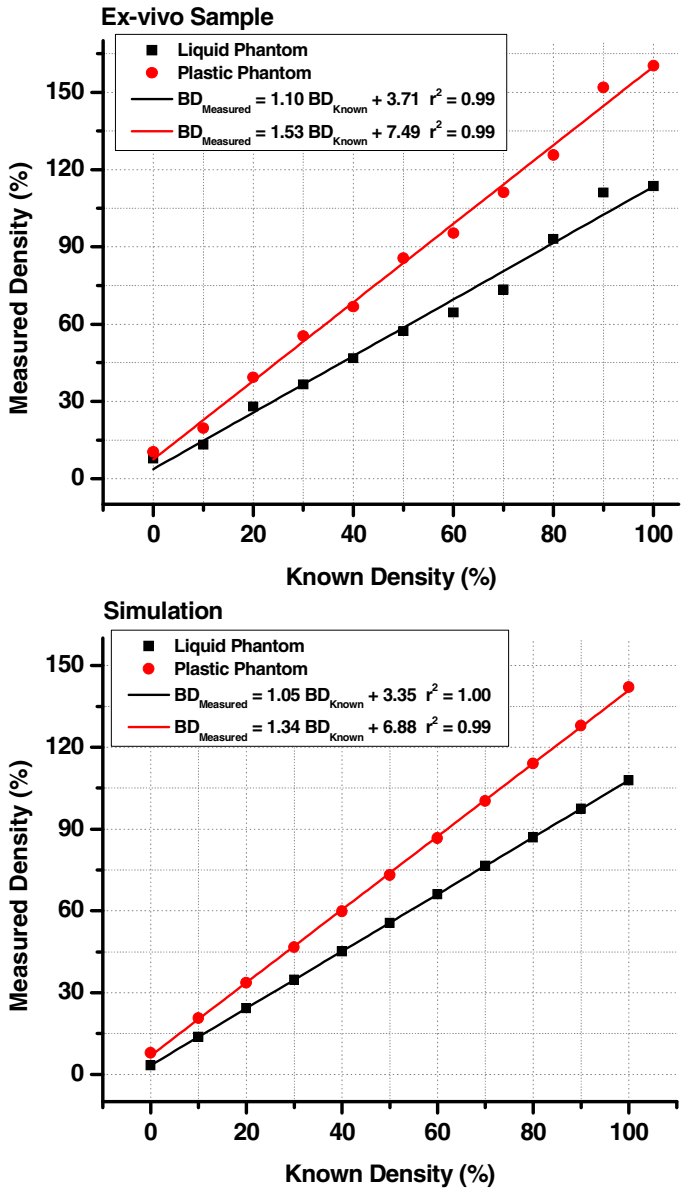

Figure 6. (a) Measured density versus known density using liquid and plastic phantoms fitting coefficients and *ex-vivo* samples with r^2 of 0.99 for both phantoms. (b) Simulation results of measured density versus known density of the skeletal muscle data with an adjusted r^2 of 1 for liquid phantoms and 0.99 for CIRS phantoms.

6. Discussion and conclusions

In this study, a dual-energy calibration technique based on liquid phantom is presented. There are a number of advantages of using liquid phantoms as compared to the existing plastic phantoms. One of the advantages is the flexibility to determine the amount of liquid compound necessary to mimic the chemical properties of any material of interest. Based on our simulation results, the predicted elemental chemical composition of the breast-equivalent

material using liquid phantom is similar to that of the reference material. Chemical composition of plastic phantoms is fixed and adapted to a specific composition. Therefore, the design of breast-equivalent materials using plastic phantoms is more restrictive as compare with liquid phantoms. Our simulation results show that a linear correlation with a slope very close to 1 can be obtained using liquid phantoms as calibration. The use of plastic phantoms, however, still provides a good linear correlation but with a slope of 0.60. On the other hand, the measured density was overestimated in both liquid and plastic phantoms because of the presence of a non-zero intercept. The presence of the non-zero intercept in the linear correlation between known and measured density can be explained by the fact that the chemical compositions of both phantoms, liquid and plastic, do not fully match with the target material and therefore differences in results were observed.

Possible explanations for this non-zero intercept value could be: (1) simplicity or non-optimal amount of the chemical elements (H, C, O). The glandular-equivalent plastic phantom shows a large discrepancy with respect to the liquid phantom. (2) Heavier elements are not present in the phantoms. Although the amounts are relatively small, discrepancies still persist. Nitrogen is not present in liquid phantoms but the extra amount of carbon and oxygen in their compositions may compensate for it. However, our simulation results show that small variations in the mass fractions can significantly alter the low- and high-energy signals. This can be seen from the perspective of the linear attenuation coefficients themselves, as shown in figure 2. The shape of the linear attenuation of the substitute material should follow similar trend as the linear attenuation curve of the reference material in the energy range considered in the study in order to maximize the accuracy to reproduce reliable calibration points.

Another advantage of using liquid phantoms is the capability to explore a wider range of thicknesses and densities, which is more restricted in plastic phantoms due to its physical configuration. In the experimental aspect, we explored several total thicknesses and densities. The results show a remarkable linear correlation between the known and measured densities when using liquid phantom for calibration, which is in good agreement with the simulation results.

It is important to point out that the slope reported by the plastic phantoms, beside the elemental chemical composition discrepancy with the target material, is also due to the fact that CIRS phantoms were originally intended to be close to the elemental chemical composition reported by Hammerstein *et al* (1979). In this study, elemental mass fractions of the glandular and adipose tissues were taken from the NIST database (ICRU-44 report), and therefore the linear correlation between measured and known densities using CIRS calibration phantom should not be expected to give a slope close to 1.

The robustness of the model allows different types of liquid that can improve the accuracy of the computed variables for the materials of interest. Thus, in theory, elemental chemical composition of a liquid phantom can be composed of other elements beside hydrogen, carbon, and oxygen. Recently, studies by Yohannes *et al* have reported tissue-equivalent phantoms based on other materials (Yohannes *et al* 2011, 2012) in CT applications.

There have been reports on the design of tissue-equivalent materials from fundamental principles (Alvarez and Macovski 1976, Brody *et al* 1981, Lehmann *et al* 1981). They have proposed that linear attenuation of any target material such as breast tissue can be modeled by combining the linear attenuations of aluminum (Al) and Lucite (PMMA), and project it in the two basis material plane where a projection vector and its projection angle carry out all the information of the target material. This technique was used to identify unknown materials, cancel out undesirable materials and enhance contrast of other materials present in the sample.

Johns and Yaffe implemented this approach to design breast tissue equivalent materials based on aluminum and Lucite (Johns and Yaffe 1987). The limitation of this approach is that

the dose applied would vary considerably due to the variations within each tissue type, and the cancellation of the projection angle in each pixel.

Liquid phantoms also have some limitations in terms of practical application. They must be stored in containers, whose chemical composition must be known, and considered in the calibration process before computing the dual-energy signals. Also, keeping unaltered chemical composition of the phantom relies on the quality of the construction of the phantoms. However, these limitations can be compensated by the fact that once the amounts of liquid materials are determined accurately to design tissue-equivalent liquid phantoms, they can be easily reproduced as needed by just making a mixture of glandular- and adipose-equivalent phantoms.

In conclusion, liquid phantoms are suitable and reliable candidates for calibration in dual-energy mammography because of their flexibility to choose a set of miscible liquids to create phantoms that closely match the chemical properties of a real tissue within the clinical applications range.

Acknowledgments

The authors would like to thank Dr Robert Jennings for helpful discussions related to liquid phantoms. This work was supported in part by NIH/NCI grant R01CA13687.

References

Alvarez R E and Macovski A 1976 Energy-selective reconstructions in x-ray computerized tomography *Phys. Med. Biol.* **21** 733–44

Boone J M and Chavez A E 1996 Comparison of x-ray cross sections for diagnostic and therapeutic medical physics *Med. Phys.* **23** 1997–2005

Boone J M and Seibert J A 1997 Accurate method for computer-generating tungsten anode x-ray spectra from 30 to 140 kV *Med. Phys.* **24** 1661–70

Boyd N F *et al* 2007 Mammographic density and the risk and detection of breast cancer *New Engl. J. Med.* **356** 227–36

Boyd N F, Lockwood G A, Byng J W, Tritchler D L and Yaffe M J 1998 Mammographic densities and breast cancer risk *Cancer Epidemiol. Biomarkers Prev.* **7** 1133–44

Brody W R, Butt G, Hall A and Macovski A 1981 A method for selective tissue and bone visualization using dual energy scanned projection radiography *Med. Phys.* **8** 353–7

Byng J W, Boyd N F, Fishell E, Jong R A and Yaffe M J 1994 The quantitative-analysis of mammographic densities *Phys. Med. Biol.* **39** 1629–38

Byng J W, Boyd N F, Fishell E, Jong R A and Yaffe M J 1996 Automated analysis of mammographic densities *Phys. Med. Biol.* **41** 909–23

Byng J W, Yaffe M J, Jong R A, Shumak R S, Lockwood G A, Tritchler D L and Boyd N F 1998 Analysis of mammographic density and breast cancer risk from digitized mammograms *Radiographics* **18** 1587–98

Byrne C 1997 Studying mammographic density: implications for understanding breast cancer *J. Natl Cancer Inst.* **89** 531–3

Ducote J, Klopfer M and Molloi S 2011 Volumetric lean percentage measurement using dual energy mammography *Med. Phys.* **38** 4498–504

Ducote J L and Molloi S 2008 Quantification of breast density with dual energy mammography: a simulation study *Med. Phys.* **35** 5411–8

Ducote J L and Molloi S 2010a Quantification of breast density with dual energy mammography: an experimental feasibility study *Med. Phys.* **37** 793–801

Ducote J L and Molloi S 2010b Scatter correction in digital mammography based on image deconvolution *Phys. Med. Biol.* **55** 1295–309

Hammerstein G R, Miller D W, White D R, Masterson M E, Woodard H Q and Laughlin J S 1979 Absorbed radiation-dose in mammography *Radiology* **130** 485–91

Heine J J and Velthuizen R P 2000 A statistical methodology for mammographic density detection *Med. Phys.* **27** 2644–51
Highnam R, Brady M and Shepstone B 1996 A representation for mammographic image processing *Med. Image Anal.* **1** 1–18
Highnam R, Jeffreys M, McCormack V, Warren R, Smith G D and Brady M 2007 Comparing measurements of breast density *Phys. Med. Biol.* **52** 5881–95
Highnam R, Pan X, Warren R, Jeffreys M, Davey S G and Brady M 2006 Breast composition measurements using retrospective standard mammogram form (SMF) *Phys. Med. Biol.* **51** 2695–713
Hubbell J H and Seltzer S M 2004 Tables of x-ray mass attenuation coefficient and mass energy absorption coefficients from 1 keV to 20 MeV for elements $Z = 1$ to 92 and 48 additional substances of dosimetric interest (version 1.4) (Gaithersburg: NIST) (http://physics.nist.gov/xaamdi)
Jennings R J 1993 Computational methods for the design of test objects and tissue substitutes for radiologic applications *Radiat. Prot. Dosim.* **49** 327–32
Johns P C, Drost D J, Yaffe M J and Fenster A 1985 Dual-energy mammography: initial experimental results *Med. Phys.* **12** 297–304
Johns P C and Yaffe M J 1985 Theoretical optimization of dual-energy x-ray imaging with application to mammography *Med. Phys.* **12** 289–96
Johns P C and Yaffe M J 1987 X-ray characterization of normal and neoplastic breast tissues *Phys. Med. Biol.* **32** 675–95
Kappadath S C and Shaw C C 2004 Quantitative evaluation of dual-energy digital mammography for calcification imaging *Phys. Med. Biol.* **49** 2563–76
Kappadath S C and Shaw C C 2005 Dual-energy digital mammography for calcification imaging: scatter and nonuniformity corrections *Med. Phys.* **32** 3395–408
Lehmann L A, Alvarez R E, Macovski A, Brody W R, Pelc N J, Riederer S J and Hall A L 1981 Generalized image combinations in dual KVP digital radiography *Med. Phys.* **8** 659–67
Lemacks M R, Kappadath S C, Shaw C C, Liu X and Whitman G J 2002 A dual-energy subtraction technique for microcalcification imaging in digital mammography—a signal-to-noise analysis *Med. Phys.* **29** 1739–51
Lu L J, Nishino T K, Khamapirad T, Grady J J, Leonard M H Jr and Brunder D G 2007 Computing mammographic density from a multiple regression model constructed with image-acquisition parameters from a full-field digital mammographic unit *Phys. Med. Biol.* **52** 4905–21
Marziani M, Taibi A, Tuffanelli A and Gambaccini M 2002 Dual-energy tissue cancellation in mammography with quasi-monochromatic x-rays *Phys. Med. Biol.* **47** 305–13
McMaster W H, Del Grande N K, Mallett J H and Hubbell J H 1969 Compilation of x-ray cross sections *Lawrence Livermore National Laboratory Report UCRL*-50174 Section II Revision 1
Pawluczyk O, Augustine B J, Yaffe M J, Rico D, Yang J, Mawdsley G E and Boyd N F 2003 A volumetric method for estimation of breast density on digitized screen-film mammograms *Med. Phys.* **30** 352–64
Shepherd J A, Kerlikowske K M, Smith-Bindman R, Genant H K and Cummings S R 2002 Measurement of breast density with dual x-ray absorptiometry: feasibility *Radiology* **223** 554–7
Sickles E A 2007 Wolfe mammographic parenchymal patterns and breast cancer risk *Am. J. Roentgenol.* **188** 301–3
Taibi A, Fabbri S, Baldelli P, Di Maggio C, Gennaro G, Marziani M, Tuffanelli A and Gambaccini M 2003 Dual-energy imaging in full-field digital mammography: a phantom study *Phys. Med. Biol.* **48** 1945–56
Wolfe J N 1976 Breast patterns as an index of risk for developing breast cancer *Am. J. Roentgenol.* **126** 1130–7
Wolfe J N, Saftlas A F and Salane M 1987 Mammographic parenchymal patterns and quantitative-evaluation of mammographic densities—a case-control study *Am. J. Roentgenol.* **148** 1087–92
World Health Organization 2006 Fact Sheet N297: Cancer
Yohannes I, Kolditz D and Kalender W A 2011 Semiempirical analysis of materials' elemental composition to formulate tissue-equivalent materials: a preliminary study *Phys. Med. Biol.* **56** 2963–77
Yohannes I, Kolditz D, Langner O and Kalender W A 2012 A formulation of tissue- and water-equivalent materials using the stoichiometric analysis method for CT-number calibration in radiotherapy treatment planning *Phys. Med. Biol.* **57** 1173–90
Zhou C, Chan H P, Petrick N, Helvie M A, Goodsitt M M, Sahiner B and Hadjiiski L M 2001 Computerized image analysis: estimation of breast density on mammograms *Med. Phys.* **28** 1056–69